Pertubations on a liquid curtain near break-up: Wakes and free edges

J. S. Roche and N. Le Grand
Laboratoire de Physique et Mécanique des Milieux Hétérogènes, UMR 7636 du CNRS, 10 Rue Vauquelin, 75005 Paris, France and Laboratoire Matière et Systèmes Complexes, UMR 7057 du CNRS, Université Paris 7, 2 Place Jussieu, 75251 Paris Cedex 05, France

P. Brunet[a)]
Laboratoire de Physique et Mécanique des Milieux Hétérogènes, UMR 7636 du CNRS, 10 Rue Vauquelin, 75005 Paris, France

L. Lebon and L. Limat
Laboratoire de Physique et Mécanique des Milieux Hétérogènes, UMR 7636 du CNRS, 10 Rue Vauquelin, 75005 Paris, France and Laboratoire Matière et Systèmes Complexes, UMR 7057 du CNRS, Université Paris 7, 2 Place Jussieu, 75251 Paris Cedex 05, France

(Received 5 May 2006; accepted 16 June 2006; published online 18 August 2006)

We report experiments on liquid curtains falling between two vertical wires. The flow is mainly driven by gravity, so that the Weber number (We) (ratio of momentum flux to twice the surface tension) is close to zero at the top of the curtain and increases downstream, with the possible existence of a location where We equals 1 (which turns out to be a singular point in the sheet, in terms of waves propagation). In the present paper, we focus on the curtain response to localized perturbations, i.e., formation of either surface waves or free edges behind a thin needle touching the curtain, with a special emphasis to what happens near the break-up limit. We extract and compare the shapes of two kind of "wakes" left behind the obstacle: classical triangular wake of standing sinuous waves and stationary hole involving two free edges pinned on the needle. It is found that these two wakes are very similar for high enough We, but behave very differently when We reaches 1 from above; the sinuous wake disappears, while the "hole wake" still exists, and its shape becomes rounded. Below We=1, the hole can either stay stable, oscillate or expand and break the curtain. We provide exact analytical expressions for stationary free-edges that compare very well with experiments. © *2006 American Institute of Physics*. [DOI: 10.1063/1.2238867]

I. INTRODUCTION

Thin liquid sheets are involved in numerous practical applications such as curtain coating,[1] atomization[2] or paper manufacturing[3] so that plane sheets falling under the influence of gravity ("curtains") have been widely studied during the last decades. Experimentally, one of the first noticeable contributions was brought on by Brown,[4] who studied the shape and stability of a curtain falling upon a moving surface (which mimics the coating processes). He suggested that a simple stability criterion could be built by comparing the momentum flux $\rho h U^2$ pushing downstream possible transient holes (ρ is liquid density, h is local curtain thickness, and U is local fluid velocity) with twice the surface tension γ, that tends to pull upstream of the hole apex. This naturally introduces the Weber number $\mathrm{We}=\rho h U^2/2\gamma$ as a key parameter for curtain stability. In other words, Brown's conclusions[4] were that the Weber number had to be larger than 1 to prevent any curtain break-up. Though it is scarcely mentioned, this conclusion can also be reached independently by comparing the liquid velocity U to the typical expansion velocity of a hole identified by Culick[5] and Taylor in the context of soap film $c_{\mathrm{exp}}=\sqrt{2\gamma/\rho h}$. The same criteria is also encountered in studies of a plane radially expanding sheet, produced by jet impingement on a solid surface (see, e.g., Refs. 6 and 7, and references therein). In this situation, the expansion radius of the sheet is also governed by a balance between inertia $\rho U^2 h$ and surface tension forces 2γ, and corresponds to a location where We=1. The application of the criteria We>1 is, however, much more conjectural in vertical liquid curtains, because contrary to the axially expanding sheet, the Weber number increases downstream. Usually, metastable states are observed near curtain break-up with a downstream stable region and an upstream unstable region, without rupture, these two regions being separated by an horizontal line where We=1, that we will call the "transonic line."[8]

Later studies of curtain stability adopted a different framework, considering that the break-up should be caused by the amplification of surface waves (considered as infinitesimal perturbations) and their spatial expansion in the sheet.[9,10] Inspired by pioneering works by Taylor,[6] these studies predicted that two types of waves can propagate on the curtain: a symmetrical mode (varicose waves) corresponding to thickness modulations, and an antisymmetrical mode (sinuous mode) corresponding to modulations of the median transverse position of the curtain.[6] These waves have the following velocities (in the limit of an inviscid ambient gas):

[a)]Present address: Department of Mathematics, University of Bristol, BS81TW Bristol, United Kingdom. Electronic mail: p.brunet@bristol.ac.uk

$$c_{\mathrm{var}} = \sqrt{\frac{\gamma h}{2\rho}}k \tag{1}$$

for varicose waves and

$$c_{\mathrm{sin}} = \sqrt{\frac{2\gamma}{\rho h}} \tag{2}$$

for sinuous waves (k being the wave number). Let us remark that the velocity of sinuous waves can be easily derived by analogy with a tight elastic membrane $c^2 = T/\mu = 2\gamma/\rho h$ where the tension $T = 2\gamma$ and mass per unit surface $\mu = \rho h$. Only varicose waves are dispersive, but they have much smaller velocities than sinuous waves in most cases. It was then usually deduced that sinuous waves are the most "dangerous" ones, in the sense that they can propagate faster than the flow velocity, i.e., upstream, and are then able to invade all of the curtain.[11] The condition for curtain stability was expressed such that the curtain should not include a $\mathrm{We} < 1$ area, so that ambient disturbances would be convected downstream. In this new framework, the conclusion is then exactly the same as Brown's. The reason why both arguments lead to the same criterion has its origin in the fact that the retraction speed of a free edge c_{exp} proposed earlier is equal to the phase velocity of sinuous waves c_{sin}.[6] More recently, the second argument, built upon the propagation of surface waves, has been renewed in terms of absolute and convective instabilities of open flows by several authors.[12,13] It is worth noticing that Sunderhauf *et al.*[14] studied the influence of viscosity and other parameters on the retraction speed: they show that the retraction speed is not constant and ranges from a zero value to the "Culick" speed c_{exp} after a time period depending on the viscosity; however such effects are shown to be expected for high enough viscosity (about 1000 cP).

In spite of the fact that the "expanding hole" and "wave amplification" approaches lead to similar stability criterion, it turns out that, at least in our specific experimental conditions, we have never observed experimental evidence of curtain break-up due to sinuous wave amplifications. In fact, repeated experiments convinced us that the curtain destruction rather results from a catastrophic amplification of a local and transient hole on the curtain; we illustrate such a process in Fig. 1, where we present the time evolution of a local perturbation; a free edge appears at the bottom, climbs up and finally invades all the curtain. We also observe on this sequence that the dynamics of free edge is quite complex and is clearly coupled to the weight of the rim formed at this free edge, i.e., to the amount of liquid collected by this rim. Obviously, the phenomenon at play during hole growth and wave propagation are in fact very different. It seemed thus important, for a complete understanding of curtain stability, to be able to compare the similarities and differences between the behavior of perturbations involving sinuous undulations on one hand and hole formation on the other hand. This remark has motivated the present study, and was already proposed in proceedings of a congress by Adachi *et al.*,[15] where a first attempt of the free-edge calculation can be found.

We provide a detailed comparison of wave effects on a curtain and their equivalents with free edges defining a hole in a curtain in the simple case of a thin needle touching the curtain (sinuous wake versus "holed wake"), with a special emphasis as to what happens near the curtain break-up limit. Intuitively, the equality $c_{\mathrm{sin}} = c_{\mathrm{exp}}$ should imply that both kinds of wakes (sinuous wake and wake formed by two free edges pinned behind the curtain) should be identical (both are the equivalent of the same "Mach cone"). However, the mechanical equilibrium of a free edge under the antagonist actions of capillarity and flow inertia should be displaced by the rim weight, so that a difference is also to be expected between the wakes. From such observations we present here a detailed study of local perturbations on the curtain; they appear to be a relevant contribution to the stability question. The role played by the rim weight is clearly significant so that it should be taken into account into the a mechanical analysis of the perturbation beyond undulatory analysis. When the gravity is not neglected, the "expanding hole" and "wave amplification" criteria are not equivalent anymore.

Thus, in the present study, localized perturbations are created by introducing an obstacle like a thin needle in the flow; this induces wave wakes, sinuous and varicose, but such an obstacle can also generate free edges ("holes"). Previous studies showed that sinuous waves downstream an obstacle appear as triangle-shaped wakes provided that the obstacle is put in the $\mathrm{We} > 1$ area.[6,9,16] Then, this area could also be called the supersonic area, identifying the velocity of sinuous waves with an equivalent of a sound velocity. These wakes, also called stationary waves in the literature, indicate that small perturbations are indeed convected downstream. In this work, we extract and compare shapes of both sinuous wakes and free edges created under similar conditions, when gravity is one of the dominant forces. This is usually the case when the curtain is about to break-up, if the flow rate is low enough. We then propose theoretical and numerical calculations of both standing waves (wakes) and free edges (holes). Several previous studies[9,16] presented theoretical and experimental results on shapes of holes and wakes; however a knowledge is lacking on their behaviors near the break-up limit, i.e., for sufficiently low flow-rates so that the curtain can suddenly break. In particular, it is usually considered that sinuous standing waves and free edges have similar behavior (this is rigorous in the absence of gravity[6]). Consequently, it is also believed that a free edge should destroy the curtain as soon as the Weber number is lower than unity. We study here these points in detail and, as we shall see, things are less simple when the rim weight is taken into account near a free edge. Beyond the determination of these shapes, our study demonstrates, at least qualitatively, the limit below which a falling curtain can withstand small and large local perturbations.

The paper is organized as follows: in Sec. II, the experiment is described and a qualitative insight of the flow is presented. Then we present first a qualitative comparison of sinuous wakes and free edges near break-up (Sec. III). Section IV reports a study of shapes of standing sinuous wakes, both calculated theoretically and extracted from experimental acquisitions. Section V reports an equivalent set of results

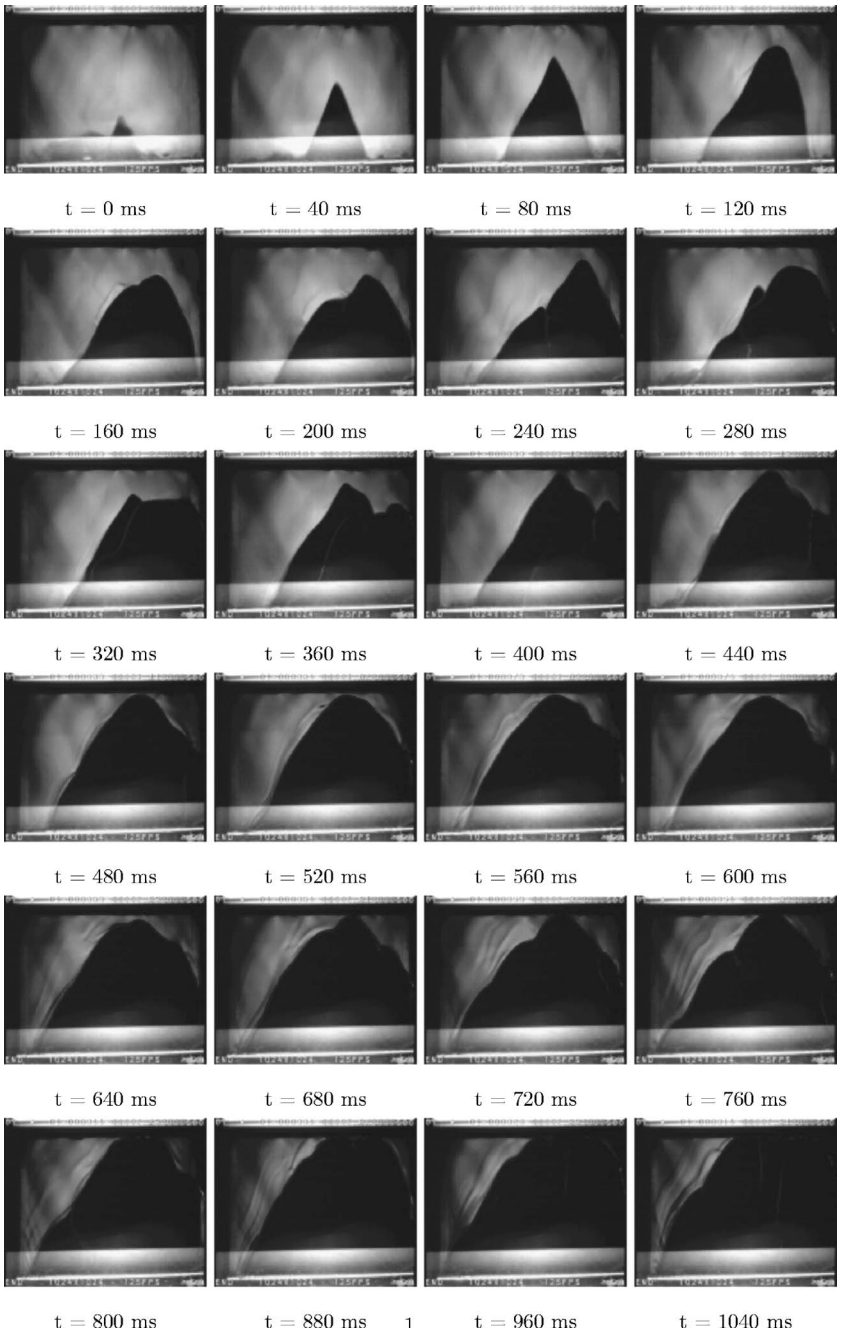

FIG. 1. A break-up screenplay: time evolution of the curtain shot by a high speed camera (125 frames per second). The dynamics of the free edge is modified by the amount of liquid collected during its climb up. Note that the time interval is changed for the four last shots in order to present the final state of the curtain (enhanced online).

for free edges, evidencing marked differences from wakes. Finally we begin to address the case of nonstationary free edges.

II. EXPERIMENTAL CONDITIONS

A. Description of the set-up

A sketch of the experiment is shown in Fig. 2. The flow is pumped from a reservoir (1), with a gear-pump *ISMATEC BVP-Z* (2) which imposes a constant flow-rate Q. A half-filled chamber (3) damps residual pulsation caused by the pump. Q is measured with a floater flow-meter (4). The liquid is then supplied to a horizontal tube through its two ends (5) (diameter $d=4.7$ or 6.8 cm). Along a generating line of this cylinder, is drilled a long thin slot (thickness $b=2$ mm, injection length of about 10 mm), from which the liquid flows. If the flow rate is sufficiently high, a liquid curtain is observed (6). Its width is 25.5 cm, and it is kept constant in the vertical direction by two thin nylon wires (diameter 0.01 cm) put under tension by two hanging weights; these wires prevent any shrinkage from capillary effects. The height of the curtain can be chosen from 15 to 25 cm. All experiments were performed with silicone oil (polydimethylsiloxane, PDMS), of different viscosities from 10 to 50 cP although most experiments presented here were run with oils of 30 and 50 cP. Table I gives the main properties of the fluids. The surface tension does is nearly the same for each and stays very low.

The liquid lies at room temperature during the experiments (between 20 °C and 22 °C). Special care is devoted to

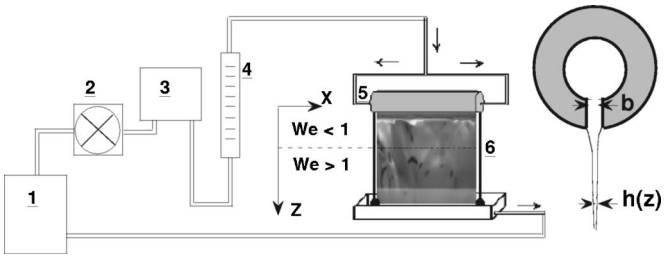

FIG. 2. Sketch of the experiment. The curtain is falling from a horizontal slotted tube and guided between two vertical threads. As suggested in the top-right inset, the slot is oriented downward.

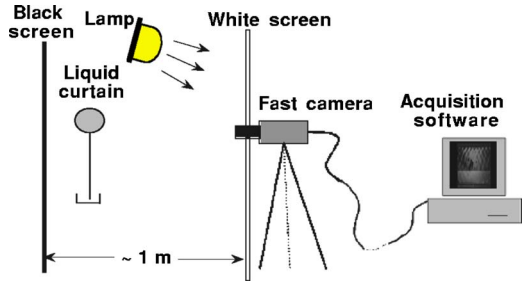

FIG. 3. Lighting and image acquisition of the curtain.

protect the system from any sources of perturbations, especially air motions around the experiment. Curtain undulations are followed by a high-speed video camera (*FASTCAM* 1024 Motion-Corder). In practice, a frequency of 250 images per second is found to be enough. Because of the required short time acquisition, it is specially important to use powerful, and nonpulsed light sources. The spatial distribution of light had also to be spatially homogeneous. The retained solution, depicted in Fig. 3, uses a 300 W incandescent lamp which lights a white screen, the latter diffusing a homogeneous light on the curtain. Another screen, black-colored, is placed behind the curtain, to maximize contrast. A circular hole was made in the white screen, whereby the camera lens fits. The reflection of this hole induces a parasite round black shadow on the pictures, of very limited extent, which does not perturb the measurements. The resulting contrast is suitable to capture clearly sinuous and varicose waves, as well as free edges.

B. Flow structure in the curtain

Before we present the experimental results, it is essential to give an insight of the flow structure and of the important parameters involved in this study; a sketch of the flow is given in Fig. 4. Regarding previous studies on falling curtains, our framework here is to study curtains that are *highly stretched by gravity*. In others terms, the Froude number $\mathrm{Fr}=gb/U_0^2$ is much larger than 1 (where U_0 is the mean velocity inside the injector). The control parameter is the flow-rate per unit width Γ, which equals $U_0 b$. Typical values of Γ are ranging between 0.2 cm^2/s and 2 cm^2/s, corresponding to values of U_0 from 1 cm/s to 10 cm/s, and Fr between 50 and 5000. The flow Weber number We_0 varies from 0.005 to 0.5. Furthermore, mass conservation implies that everywhere in the curtain,

$$\Gamma = Uh. \tag{3}$$

As emphasized in previous studies,[4,9,13] the velocity field reads

$$U^2 = U_0^2 + 2g\left[z - 2\frac{(4\nu)^{2/3}}{g^{1/3}}\right]. \tag{4}$$

Brown[4] first introduced this viscosity dependent term $2(4\nu)^{2/3}/g^{1/3}$. Deduced from experimental measurements it quantifies the effect of the transition from a Poiseuille flow at the nozzle exit, to a plug flow in the bulk of the curtain. The mechanisms of this transition are not trivial but according to theoretical and experimental results,[3,18,19] the velocity field becomes constant in the y direction when z is larger than a length comparable to the thickness of the slot. The plug flow is clearly a first order approximation since the curtain thickness h varies along z.

In our experimental conditions the corrections can be neglected as soon as the distance from the slot is higher than a few millimeters

$$\frac{U_0^2}{2g} \approx 0.3 \text{ mm} \quad 2\frac{(4\nu)^{2/3}}{g^{1/3}} \approx 1 \text{ mm}. \tag{5}$$

Finally the flow is well approximated by a simple free-fall

$$U^2 = 2gz. \tag{6}$$

This has been checked experimentally by measuring the angle of a sinuous wake below an obstacle, using the method exposed in Ref. 9. More evidence for the validity of (6) will be given in the next section, by observing the z^* coordinate

TABLE I. Physical properties of liquids.

Liquid ref.	Kinematic viscosity ν (mm^2/s)	Surface tension γ (dyn/cm)	Density ρ (g/cm^3)
PDMS 47V10	10.3	20.1	0.935
PDMS 47V30	32.0	20.4	0.947
PDMS 47V50	53.6	20.4	0.957

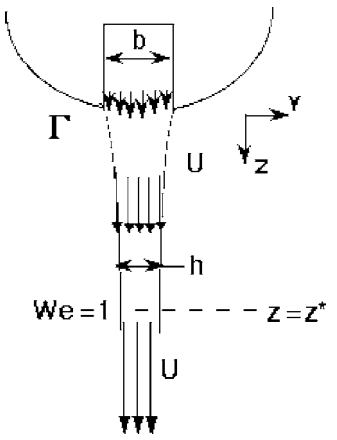

FIG. 4. Cross-sectioned view of the flow and shape of the curtain.

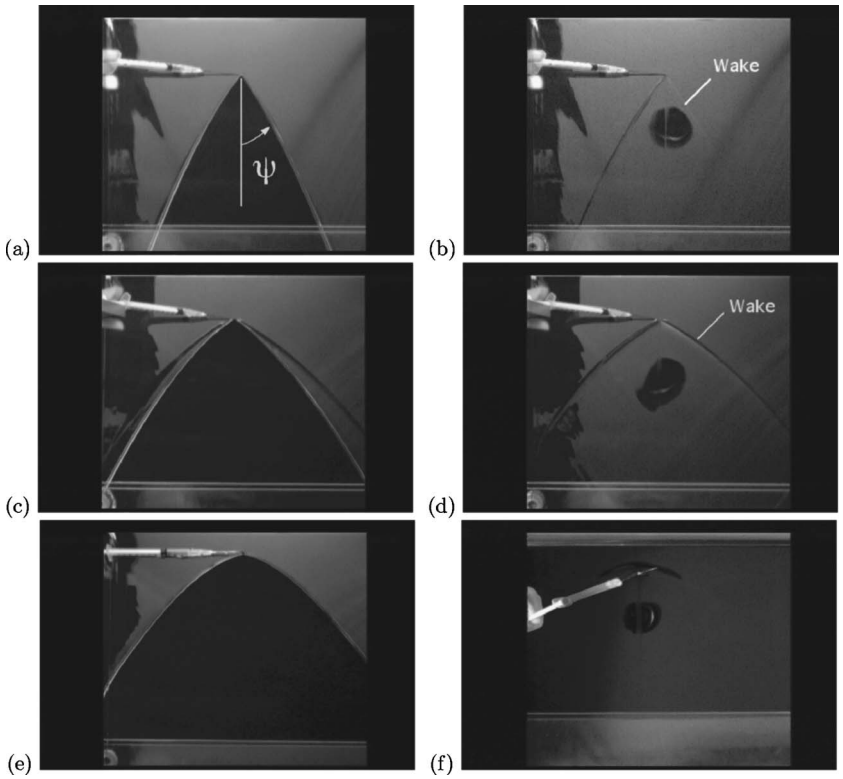

FIG. 5. Response of the curtain to a needle for a 50 cP silicone oil. (a) Nonwetting needle, $\Gamma=1.54\ \mathrm{cm^2\ s^{-1}}$, $z_0=5.0$ cm, We=3.50; (b) same values but with a wetting needle. (c) Non-wetting needle, $\Gamma=0.65\ \mathrm{cm^2\ s^{-1}}$, $z_0=3.5$ cm, We=1.25; (d) same values but with a wetting needle. (e) Non-wetting needle, $\Gamma=0.56\ \mathrm{cm^2\ s^{-1}}$, $z_0=2.1$ cm, We=0.84; (f) wetting needle, $\Gamma=0.56\ \mathrm{cm^2\ s^{-1}}$, $z_0=3$ cm, We=1.01. We can observe a small vertical wake in (b), (d), and (f) just under the needle: this is the wake of the varicose waves that travel at very low velocities. Note that the black circle in (b), (d), and (e) is an artifact resulting from the camera reflecting on the liquid curtain.

above which sinuous wakes disappear, versus flow-rate. Equation (6) implies that neither the flow-rate nor the viscosity influences the velocity field in our experiments. However, the flow-rate is linked to the sheet thickness h by (3), so that the Weber number reads

$$\mathrm{We}=\frac{\rho\Gamma U}{2\gamma}. \tag{7}$$

This suggests, on the one hand, that We starts from a value much smaller than one at the top of the curtain (chosen as $z=0$) and increases downstream as $\sim(z)^{1/2}$. On the other hand, an increase/decrease of the flow-rate will increase/decrease globally We and then allow to control the position of the transonic line at $z=z^*$:[20]

$$z^*=\frac{2\gamma^2}{\rho^2 g\Gamma^2}. \tag{8}$$

Also, in such conditions, we can observe a stable curtain, with a large subsonic area ($\mathrm{We}<1$). The length of this area is easily measurable as already noticed by De Luca;[13] it is simply the upstream area above the coordinate z^*.

III. QUALITATIVE COMPARISON OF SINUOUS WAKES AND FREE EDGES

We have perturbed the curtain by touching it with a thin needle, varying the flow rate and the needle position. Depending on the way we approach the curtain, rupture can occur or not; it is illustrated in Fig. 5. The perturbation can just lead to surface waves of small amplitude [Figs. 5(b), 5(d), and 5(f)] or it can become finite, tearing the curtain and a free edge would develop downstream [Figs. 5(a), 5(c), and 5(e)] [let us note that the black circle in Figs. 5(b), 5(d), and 5(f) is an artifact resulting from the camera reflecting on the curtain]. Let us call z_0 the position of the obstacle (the origin of the perturbation); the corresponding Weber number is We.

At $\mathrm{We}>1$, the two kinds of perturbations can coexist; if the perturbation is weak enough, for example induced by a thin (size of the order of 1 mm) and wetting needle, we observe a standing wake downstream the obstacle [Fig. 5(b)]. The shape of the wake can easily be predicted by a Mach cone construction as it is usually done for supersonic flows; in the frame of the liquid, the needle moves at a speed U higher than that of the sinuous waves. In our case, the wake is curved since both velocities U and c are not uniform and depend on the local position z.[9]

For a stronger perturbation, we observe the formation of a free edge expanding on the curtain as illustrated in Fig. 5(a). The free edge is stable for such We and stays trapped by the needle. The liquid is collected into a thick rim. The shape of the rim seems to depend on the viscosity;[14] our experimental conditions lead to a rim the characteristic length of which is of order 0.1 cm (so 10–100 times larger than the curtain thickness). The comparison between wakes with and without a hole reveals that the hole does not influence the shape of the wake (see Fig. 5). This observation is consistent with the fact that any local perturbation applied at $\mathrm{We}\geqslant 1$ is washed downstream and therefore information cannot travel upwards.[17] For high enough We, the wake and the free edge seem merged.

When we reduce We, the wake and the free edge become clearly distinct [Fig. 5(c)]. This is evidence that the weight of the rim gathering the liquid flowing down from the sheet has to be taken into account to predict the free edge shape. The lower the Weber number becomes, the stronger the liquid

weight plays a role in the mechanical balance while the role of inertia decreases.

However the opening angle ψ of the wake and the free edge at the origin are identical while the weight is still negligible at the beginning of the rim. This can also be easily understood by the fact that the sinuous wave velocity is equal to the inertial dewetting velocity; the latter describes the motion of a weightless free edge. Far from the origin, the liquid flowing from the curtain weighs the rim down and therefore tends to increase its bend so that the free edge shape is more closed than the wake.

The effect of the rim weight appears more radically when We is further decreased, as illustrated in Figs. 5(e) and 5(f). At We smaller than unity, the sinuous wake disappears since sinuous waves travel faster than the liquid (subsonic regime). On the contrary, the free edge still exists with a parabolic apex ($\psi=\pi/2$).

At this level, it is now possible to draw some conclusions from these primary observations. Obviously in the presence of gravity the mechanical equilibrium of the rim is not only governed by the counterbalancing effects of inertia and surface tension (this equilibrium predicts that the hole should expand at $We<1$). The physics, then, are slightly more complex than for the flat sheets studied by Taylor,[6] where the weight of the rim was not involved in the balance. Here, the weight seems to bring a stabilizing effect, so that a free edge can be withstood until the Weber number equals approximately 0.7.

In the next sections, we provide detailed theoretical studies of the wake and free edge shapes as a function of the Weber number.

IV. SHAPE OF THE SINUOUS WAKE BELOW AN OBSTACLE

As previously expressed, when the obstacle is perfectly wetted by the liquid, it constitutes a local source (from a point situated at $z=z_0$) of antisymmetric surface waves that propagate in the curtain at $c_{\sin}$. Previous experiments,[13] as well as our own verifications, showed that the wake angle is not dependent on the size of the obstacle. These waves are simultaneously convected by the flow at the velocity U so that the shape of the wake is ruled by the competition between these two velocities. We give here a analytical expression of the shape of the wake as previously reported in Refs. 9 and 16. The final relation we provide here, explicitly contains the parameters we vary in our study. We focus here on the behavior of the wake at low We near the transonic point. We shall also see in this calculation that a kinematic description allows us to predict the wake shape, contrary to the case of the hole that is treated in the next section.

A kinematic argument leads to a relation between the sine of half the summit angle [$\psi(z_0)=\theta/2$] and the ratio between the speed of the wave and the speed of the flow. As this ratio $c_{\sin}/U$ is dependent on z, the wake is a curved line (Fig. 5).

The quantity $\psi(z)$ is the angle between the vertical axis and the tangent to the wake curve at z:

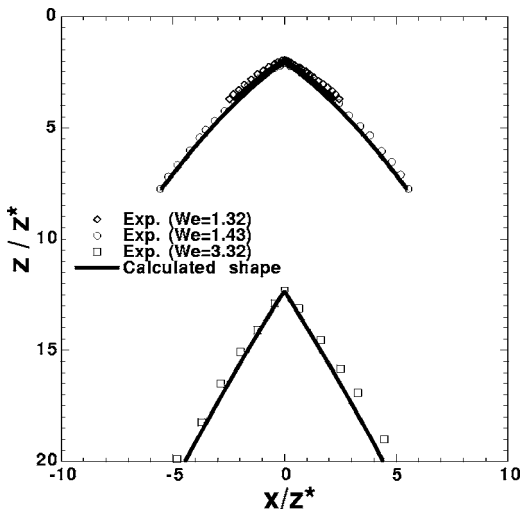

FIG. 6. Compared experimental and calculated shapes for sinuous wakes. (1) $\Gamma=0.47$ cm^2/s, $z_0=8.20$ cm (We=1.32). (2) $\Gamma=0.71$ cm^2/s, $z_0=3.92$ cm (We=1.43). (3) $\Gamma=1.54$ cm^2/s, $z_0=4.93$ cm (We=3.35). $\eta=30.3$ cP.

$$\sin\psi=\frac{dr}{dz}=\frac{c(z)}{U(z)}=\left(\frac{2\gamma}{\rho\Gamma(2gz)^{1/2}}\right)^{1/2}=\tilde{z}^{-1/4}, \tag{9}$$

where $\tilde{z}=z/z^*$ is normalized by the transonic length z^* [Eq. (8)]; $\tilde{x}=x/z^*$. Straightforwardly, the differential equation governing the shape of the wake $\tilde{z}(\tilde{x})$ reads

$$\left(\frac{d\tilde{z}}{d\tilde{x}}\right)^2=\sqrt{\tilde{z}}-1. \tag{10}$$

An integration gives the following equation for the wake:

$$\tilde{x}(\tilde{z})=\pm\frac{4}{3}(\sqrt{\tilde{z}}-1)^{1/2}(\sqrt{\tilde{z}}+2)+\tilde{x}_0, \tag{11}$$

with

$$\tilde{x}_0=\mp\frac{4}{3}(\sqrt{\tilde{z}_0}-1)^{1/2}(\sqrt{\tilde{z}_0}+2) \tag{12}$$

(the + and − signs stand, respectively, for the half-part of the wake corresponding to $x>0$ and $x<0$ if $x=0$ is chosen as the needle position).

We can remark that this known result is consistent with the prediction of the wake shape calculated on a three-dimensional inviscid curtain by Weinstein *et al.*[21]

In Fig. 6, we compare calculated and experimental shapes at lower We for different conditions, emphasizing that We is the relevant quantity to characterize the shape. Indeed, at different conditions on z_0 and Γ, shapes are similar provided that there is the same We at the obstacle location. In Fig. 6, shapes at We=1.43 and We=1.32 are almost similar, the latter being slightly more open.

Experimental measurements on wake angles versus the vertical coordinate of the obstacle are reported in Fig. 7(a), for different flow-rates. For each flow-rate, there exists a value of z for which the half-angle of the wake summit

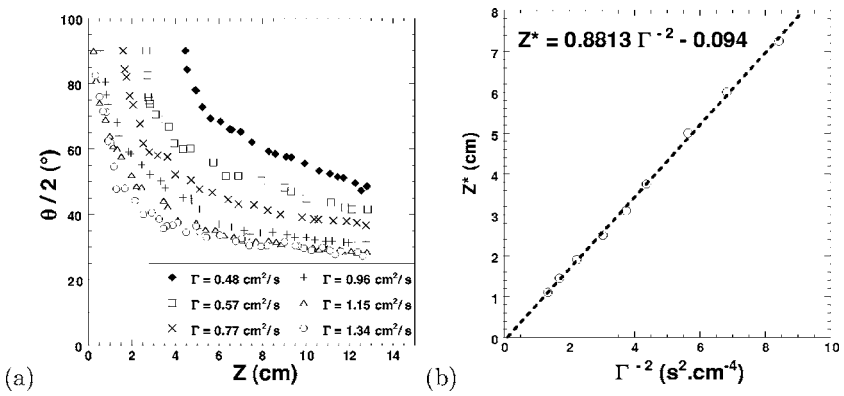

FIG. 7. (a) Evolution of the wake angle at apex with z, for different flow-rates. (b) Vertical coordinate above which the sinuous wake disappear, the dotted line is a linear fit.

reaches 90° after a sharp variation. This corresponds to the position of the transonic line as defined earlier in Eq. (8), where We=1.

The position of z^* has been measured for several flow-rates. These results are reported in Fig. 7 showing a good agreement with Eq. (8). The prefactor $(2\gamma^2/\rho^2 g)$ equals 0.940 $cm^5\ s^{-2}$, and the experimental fit gives a close value of 0.864 $cm^5\ s^{-2}$. As expected this validates the simple free-fall flow assumed in Eq. (6).

V. SHAPE AND STABILITY OF A HOLE BELOW AN OBSTACLE

Practically, the hole is created by the same kind of needle as previously, but taking care to keep it dry before introducing it through the curtain. However, the comparisons between free edges and wakes, presented in Sec. III, showed that the similarity is only qualitative. First, the liquid is collected into a thick rim surrounding the hole; second, the hole and its companion wake have different shapes when the Weber number is close to one (Fig. 5); then, at We$<$1, it is possible to observe the hole while the wake has vanished.

A purely kinematic argument based on the comparison between the speed of the flow and the one of the wake/hole expansion [i.e., Eq. (9)] leads to similar shapes for both objects. The observed differences are then presumably consequences of the weight of the rim which adds a force in the downstream direction. Most previous studies did not take into account the weight of the rim; this effect was indeed negligible there, because either the sheet was formed in the horizontal plane;[6] either We was much larger than one so that inertia forces pushed sufficiently strongly on the rim to mask the influence of the weight of the rim.[9] Then it was usually concluded that sinuous wakes and holes have the same shapes. We present a calculation of the shape of a free edge that includes this force.

Let us recall that Adachi *et al.*[15] proposed such a calculation, applied to side free edges of the curtain without guide. It is based on the mass and momentum balances on the rim. However several aspects of their model are problematic. First, the choice of the initial conditions at the top of the free edge is not justified in their paper; it may fit the case of the side free edge, but it is not relevant to our experimental situation of a free edge below an obstacle in the middle of the curtain (particularly, it leads to a different shape for We$>$1). Secondly, they made an arbitrary and restricted assumption on the shape of the rim; it is assumed to be circular. In fact the real shape is not circular and strongly depends on the fluid characteristics (viscosity, density, and surface tension).[14] Furthermore, the calculation presented thereafter demonstrates the influence of the weight on the stability of the free-edge.

A. Calculation of the shape of a free edge

The difference between the derivation of the equation for the wake in an unbounded curtain and that of a free edge, both involving the solution of momentum equations, is the accounting of the mass accumulation in the free edge. Geometrical definitions are the same as previously; we introduce here the curve-abscissa s along the rim. The shape of the hole itself is represented by the function $x(z)$.

The conservation laws are applied through the surface Σ, as shown in Fig. 8. Σ is bounded by the two disks Σ_1 and Σ_2, respectively, at the abscissa s and $s+ds$ and by Σ_L, which is the lateral surface of the pseudocylinder intercepting Σ_1 and Σ_2. As suggested in Fig. 8, the x axis origin is chosen at the hole apex, whereas the z axis has its origin at the top of the curtain. The summit coordinates are then $(0, z_0)$. $(\mathbf{e}_N, \mathbf{e}_T)$ define a convenient local framework, with the normal and tangent (to the rim) unitary vectors.

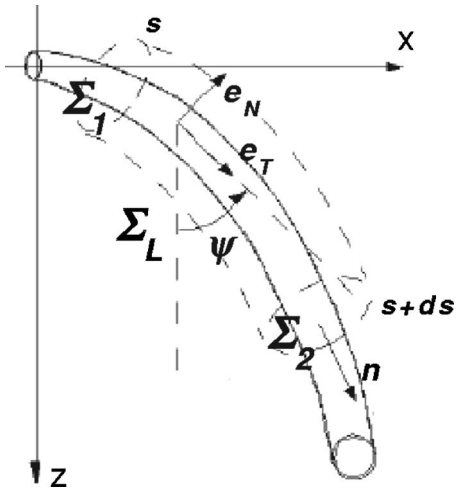

FIG. 8. Definition of the control surface for forces equilibrium. $(\mathbf{e}_N, \mathbf{e}_T)$ is the local framework.

The angle between the vertical and the tangent axis is denoted Ψ.

The geometrical parameters of the rim are defined by:

- V, for the liquid velocity inside the rim.
- S, for the rim section.
- l_r, for the rim perimeter of order $\sqrt{S}$.

All these quantities depend on s.

The mass conservation between the curtain and the rim leads to

$$\Gamma x = SV. \tag{13}$$

This relationship simply reflects that the fluid which does not lie in the hole area, is captured in the rim.

At this stage, it is necessary to make some assumptions, based on experimental observations: first, we consider that the curtain upstream the free edge is not perturbed by the rim, which has been suggested by the observations of similar shapes of wakes with or without a hole (see Fig. 5). Secondly, it is assumed that the velocity inside the rim is uniform, and follows the direction of $\mathbf{e}_T$. This means that the thickness of the transition zone from curtain to rim would be much less extended than the thickness of the rim, which is realistic, considering that the curtain is much thinner than the rim. It is worth noticing that these assumptions are supported by the following observation: if a small amount of colored oil (covering a few square millimeters on the sheet surface) is dropped on top of the curtain, it falls vertically until it reaches the edge of the hole, then it enters the rim and follows the flow along it until the bottom of the curtain.

In the general form, a momentum conservation applied to the open surface Σ reads

$$\left.\frac{d\mathbf{p}}{dt}\right|_{\Sigma} = \sum \mathbf{F} - \oint_{\Sigma} \rho \mathbf{v}(\mathbf{n}_{\Sigma}\mathbf{v}) d\Sigma. \tag{14}$$

The integral term holds for the momentum flux through Σ, and $\Sigma\mathbf{F}$ represents forces applied to the liquid volume bounded by Σ. These forces come from

- the weight of the rim $\rho g S ds \mathbf{e}_z$, submitted to gravity;
- the surface tension force on the sheet: $2\gamma ds \mathbf{e}_N$;
- the surface tension acting along the rim: $\gamma l_r \mathbf{e}_T|_{s+ds} - \gamma l_r \mathbf{e}_T|_s = \gamma (dl_r \mathbf{e}_T/ds) ds$.

From Eq. (A1), this can be transformed and projected on the framework axis $(\mathbf{e}_T, \mathbf{e}_N)$ as illustrated in Fig. 9(a):

$$\sum \mathbf{F} \cdot \mathbf{e}_T \frac{1}{ds} = \rho g S \cos \Psi + \gamma \frac{dl_r}{ds}, \tag{15}$$

$$\sum \mathbf{F} \cdot \mathbf{e}_N \frac{1}{ds} = -\rho g S \sin \Psi + 2\gamma + \gamma l_r \frac{d\Psi}{ds}. \tag{16}$$

Figure 9(b) describes the momentum variations due to mass exchange through Σ:

- through Σ_1: $\rho V^2 S \mathbf{e}_T|_s$.
- through Σ_2: $-\rho V^2 S \mathbf{e}_T|_{s+ds}$.
- through Σ_L: $\rho h U^2 \sin \Psi ds \vec{e}_z$.

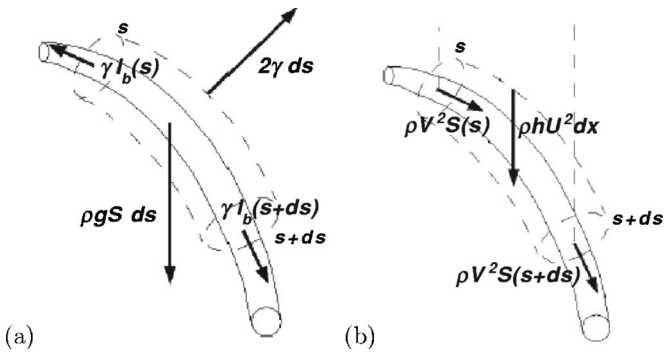

FIG. 9. (a) Local equilibrium of forces on the rim. (b) Local momentum conservation due to mass exchange.

We search for stationary solutions; details of the intermediate calculation can be found in the Appendix. The equations governing the shape of the free edge finally read

$$\begin{aligned} &-\rho \frac{dSV^2}{ds} + \rho h U^2 \sin \Psi = \rho g S \cos \Psi + \gamma \frac{dl_r}{ds}, \\ &-\rho S V^2 \frac{d\Psi}{ds} - \rho h U^2 \sin^2 \Psi = -\rho g S \sin \Psi + \gamma l_r \frac{d\Psi}{ds} + 2\gamma. \end{aligned} \tag{17}$$

In order to pursue the resolution of this system of equations, other assumptions are necessary, justified by estimations of orders of magnitude; we consider the rim as a slender body, neglecting its thickness in comparison to the spatial extension of the hole, but we do not neglect its weight. This assumption is questionaby very close to the hole summit. However the obstacle introduces an end effect on the same order as the rim thickness, and thus, these assumptions are consistent with the neglect of the end effect; we will come back later on this point. Using this assumption and the mass balance [Eq. (13)], we obtain as detailed in the Appendix

$$\frac{\rho g \Gamma^2}{2\gamma} \frac{x^2}{z - z_0} \sin \Psi + \Gamma U \sin \Psi = \frac{2\gamma}{\rho} \frac{d}{dz} \left(\frac{z - z_0}{\sin \Psi} \right). \tag{18}$$

Using the normalized length, it reads

$$\frac{d^2 \tilde{z}}{d\tilde{x}^2} = \frac{\tilde{x}^2}{2(\tilde{z} - \tilde{z}_0)^2} + \frac{\sqrt{\tilde{z}}}{\tilde{z} - \tilde{z}_0} - \frac{1}{\tilde{z} - \tilde{z}_0} \left[1 + \left(\frac{d\tilde{z}}{d\tilde{x}} \right)^2 \right]. \tag{19}$$

Here all the lengths are normalized by the transonic length z^*: $\tilde{z} = z/z^*$, $\tilde{z}_0 = z_0/z^*$, and $\tilde{x} = x/z^*$.

B. Integration of the free edge shape

The resolution of Eq. (19) needs two boundary conditions. One of these is obvious: $\tilde{z}(\tilde{x}=0) = \tilde{z}_0$. The second condition is chosen considering the following: let us remark that several terms containing $1/(\tilde{z} - \tilde{z}_0)$ diverge for $\tilde{z} = \tilde{z}_0$ (which can lead to the divergence of $d^2\tilde{z}/d\tilde{x}^2$). While the term $\tilde{x}^2/2(\tilde{z} - \tilde{z}_0)^2$ remains bounded in the vicinity of $\tilde{z}_0$ (as $\tilde{x}$ is then proportional to $\tilde{z} - \tilde{z}_0$), the other terms will have to cancel each other at $\tilde{z}_0$ to prevent the divergence:

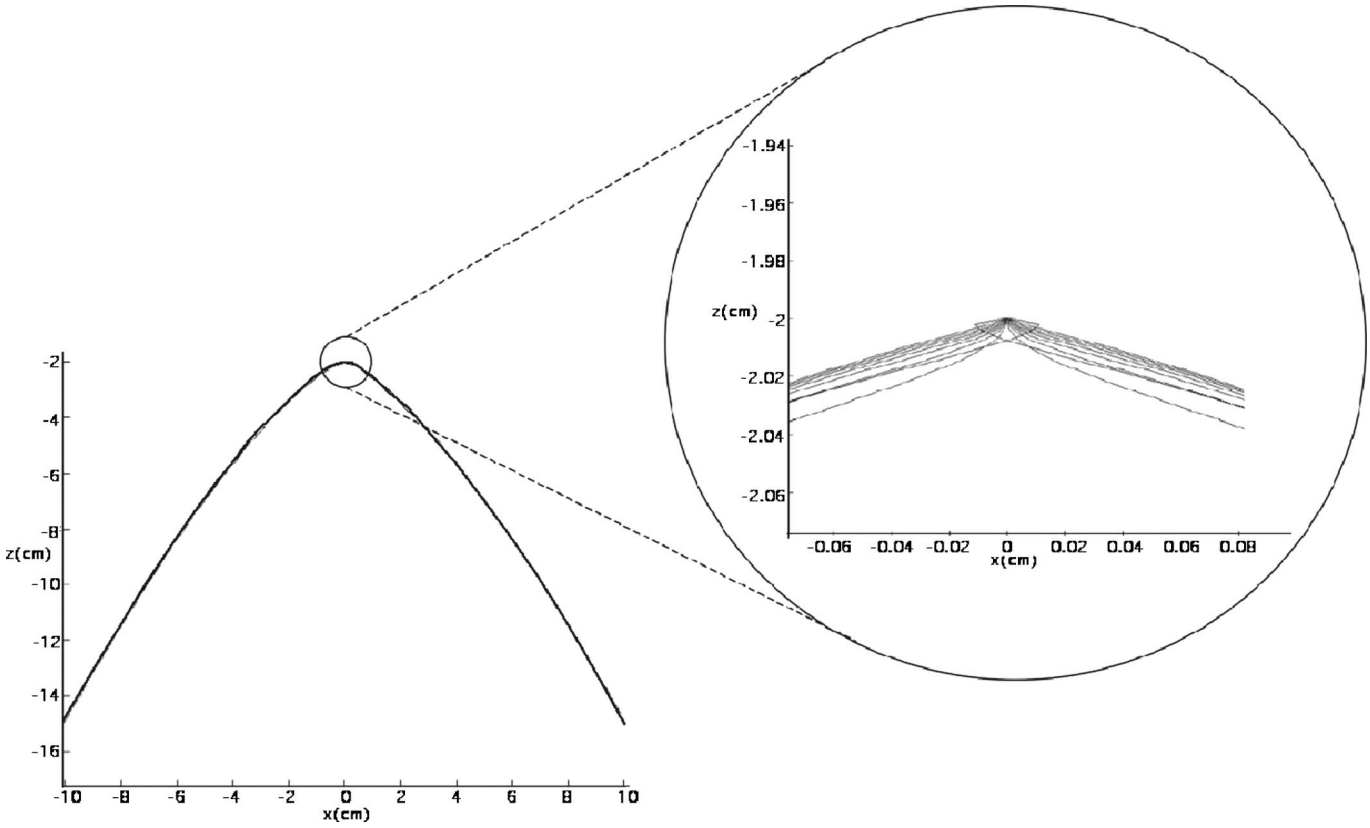

FIG. 10. Calculated shape of a free edge from Eq. (19) (η=31.3 cP, Γ=0.7 cm^2/s, z_0=2 cm, We=1.02) and detailed view near the summit for different values of the initial angle.

$$\left[\sqrt{\tilde{z}}-\left(1+\left(\frac{d\tilde{z}}{d\tilde{x}}\right)^2\right)\right]_{\tilde{x}=0}=0$$

so that we finally obtain an initial condition for the angle of the free edge at the origin:

$$\left.\frac{d\tilde{z}}{d\tilde{x}}\right|_{\tilde{x}=0}=\pm\sqrt{\sqrt{\tilde{z}_0}-1}. \tag{20}$$

Of course, such an expression is valid for $z_0 \geqslant z^*$ corresponding to We$\geqslant$1. In this case, the angle at the origin is exactly the same as the one corresponding to the wake, see Eq. (10). This means that, very close to the obstacle, the angle of the hole and the one of the wake are equal. This is experimentally realistic (the shapes differ from each other only further downstream) and it physically means that the weight of the rim is locally neglected near z_0. Let us remark here that this initial condition is fully consistent with the calculation performed by Antoniades *et al.*;[22] they used the value for the initial angle of a hole to measure dynamic surface tension.

When the Weber number approaches 1, the angle at the apex ψ approaches $\pi/2$. We observed that free edges in the subsonic area present a parabolic shape; thus, for We$\leqslant$1, we choose

$$\left.\frac{d\tilde{z}}{d\tilde{x}}\right|_{\tilde{x}=0}=0. \tag{21}$$

To solve Eq. (19) with the two boundary conditions (20) or (21), we use a variable step algorithm provided by the Matlab package. The results of such calculations and their comparisons to experiments are presented in the next subsection. Let us note that in practice any arbitrary choice of the initial angle does not change the "macroscopic" initial angle obtained by the calculation as illustrated in Fig. 10; at a very small scale, the calculated shape will converge rapidly to the physical values of the initial angle as proposed by Eq. (20) or (21), whatever its imposed initial value.

Note that for We$\leqslant$1, it was necessary to run the calculation starting at a finite value for $(z-z_0)$, of the order of 0.1 mm corresponding to a fraction of the needle thickness; this disables the calculation to diverge. Of course, the result does not depend on the arbitrary choice of the length provided it stays small. This is consistent with the cut length observed around the needle; a very tiny rim of liquid surround the needle.

C. Comparison with experimental shapes

Comparisons between experimental shapes and numerical calculations of Eq. (19) show very good agreement. Figures 11(a)–11(c) provide three examples, at We larger than, near, and smaller than 1. The dotted white curve is the calculated shape and the experimental shape is visible as a clear track due to light reflection on the rim. The thickness of the rim is also visible, and it appears that the discrepancy be-

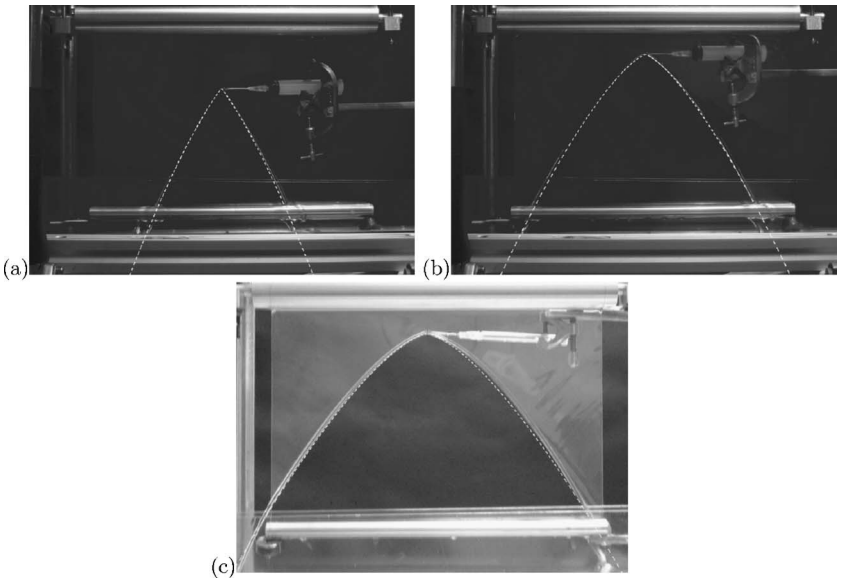

FIG. 11. Comparison between experimental and calculated shapes [from Eq. (19)] of a hole below an obstacle. η=31.3 cP. (a) We=2.76; (b) We=1.07; (c) We=0.77.

tween calculated and experimental shapes is of the order of this thickness; the prediction of the shape is thus very satisfactory.

Let us remark here that we made the assumption of a very simple velocity field in the curtain [see Eq. (6)]. No particular correction of this free fall velocity is needed to correctly predict the shape of the free edge. Similarly, it is not necessary to make particular assumption on the shape of the rim to describe the free edge.

D. The limit of stability of a hole: Oscillations and break-up of the curtain

We report here first observations of unstationary free edges (Fig. 12). At lower We (in a range of value around 0.7 with a few percentage accuracy), the obstacle generates an oscillating hole. This phenomenon is robust, as it was possible to observe such oscillations up to 2 h.

The mechanism of these oscillations is not obvious, but

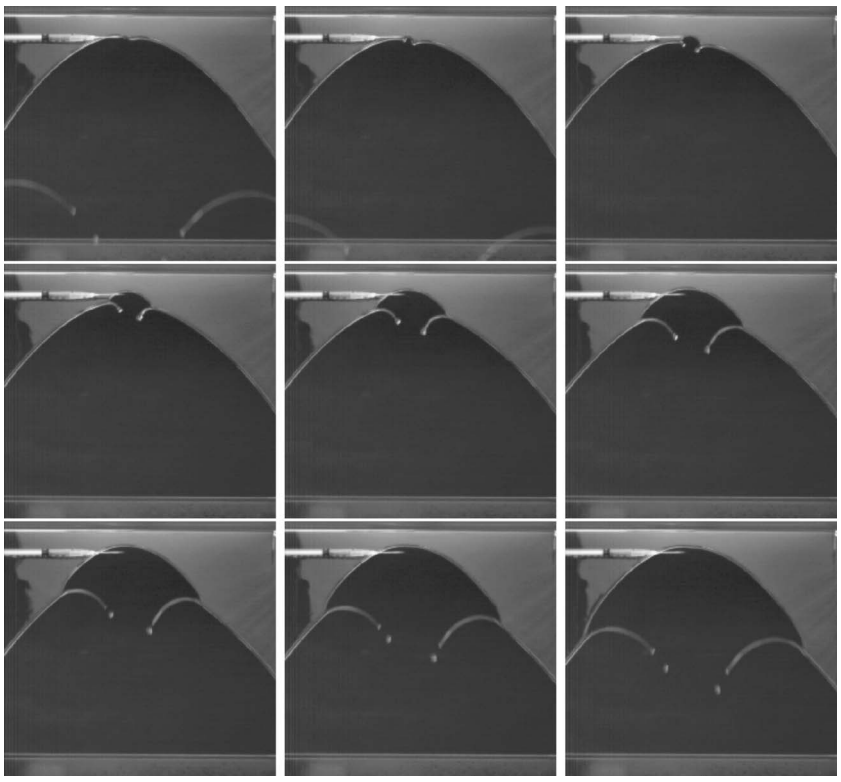

FIG. 12. Successive snapshots of an oscillating hole at We=0.69. η=51.3 cP, z_0=1.92 cm, and Γ =0.51 cm^2/s. Shots are taken every 20 ms.

we can give here the following qualitative picture. It is shown that some specific conditions (mainly the value of We) make the free edge detach from the needle, and start expanding upstream. The rim catches more liquid and then becomes heavier, so that this additional weight acts against surface tension and tends to push the hole downstream, until it touches the needle again. Then, the rim breaks (Figs. 12 would suggest that the rim is pealed) and becomes lighter, so that the force of the rim weight decreases and oscillations go on.

Nevertheless, it has not been possible to extract any reproducible measurements of the frequency, which seems to be very sensitive to experimental conditions. Despite the good accuracy with which the position of the needle in the flow-rate can be controlled (respectively, ±0.1 mm and ±0.01 cm^2/s), we measured frequencies with variations of 100% (in a typical range of 2–5 Hz) for two different acquisitions with apparently similar conditions.

At $We < 0.7$, the hole is pulled upstream by surface tension effects, and leads to the break-up of the curtain. The latter is then replaced by an array of liquid jets. A new curtain can be created again on the condition that the flow-rate per unit length is increased again up to 5 cm^2/s. This hysteretic behavior seems to be an essential property of liquid curtains, which generally need finite perturbations to be broken.

VI. DISCUSSION AND CONCLUSIONS

The set of experiments reported here offers an overview of curtain responses to local disturbances. We tested the curtain reaction to both weak and strong perturbations, corresponding, respectively, to waves and waves+holes, depending on the local We.

Our study provides a set of experimental shapes of sinuous wakes and holes for a curtain flow mainly driven by gravity (small flow-rates), and provides calculations that compare well with experiments. Our model for the free edge does not require specific corrections for the velocity field in the curtain. It does not require either specific or unnecessary assumptions on the rim shape. These results clearly illustrate that even though sinuous waves and holes have similar shapes and velocity, differences between the two objects are visibly close to $We=1$. A free edge is seemingly stabilized by the weight of its own rim, and so can still exist down to $We \simeq 0.7$ without expanding. Around this value, a spectacular oscillatory behavior is observed, confirming the influence of the rim weight.

Our results show that the predicted limit of $We=1$ is usually overcome. Sinuous waves brought by obstacles are borne by the curtain, even if the flow is entirely subsonic. Observations of stable steady-state curtains with very low Weber number was previously reported;[13,20] here such a stable subsonic curtain is observed even if we generate perturbations (see Fig. 13).

This study should then be related to the still unsolved problem of the falling curtain stability. First, the stability criterion by Brown[4] fails: holes do not necessarily expand for $We<1$ and they can spontaneously heal if the obstacle is removed. Secondly break-up scenarios from wave amplification predicted by linear analysis[9,10,12,23] appears useless here. As we observed that a needle put through an entirely subsonic curtain does not break it (see Fig. 13 and online movie, although generating both sinuous and varicose waves), it shows that such an analysis somehow does not succeed in giving a relevant criterion for break-up for our experimental conditions. Such observations are in agreement with conclusions drawn theoretically.[24] Even if one cannot completely exclude a break-up scenario involving the growth of waves, one has to keep in mind that break-up would imply that the curtain has to thin locally to molecular thickness,[20] which overcomes the framework of linear analysis.

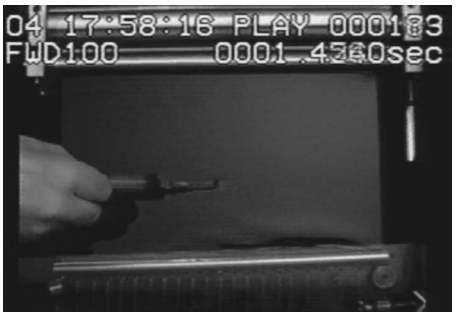

FIG. 13. A needle that bring perturbations to an entirely subsonic curtain (the Weber number ranges from 0 at the top to 0.6 at the bottom). Although the curtain is perturbated, it stays stable (enhanced online).

APPENDIX: DETAILED CALCULATION OF THE SHAPE OF A FREE EDGE

First, we present some useful geometrical relations:

$$\frac{d}{ds} = \frac{dz}{ds}\cdot\frac{d}{dz} = \cos\Psi\frac{d}{dz},$$

$$\frac{d\mathbf{e}_T}{ds} = \frac{d\Psi}{ds}\mathbf{e}_N = \cos\Psi\frac{d\Psi}{dz}\mathbf{e}_N = \frac{d\sin\Psi}{dz}\mathbf{e}_N, \tag{A1}$$

$$\mathbf{e}_z = \cos\Psi\mathbf{e}_T - \sin\Psi\mathbf{e}_N.$$

The tangential and normal components of the momentum flux through Σ read

$$-\oint_\Sigma \rho\mathbf{v}(\mathbf{n}_\Sigma\cdot\mathbf{v})d\Sigma\frac{\mathbf{e}_T}{ds} = -\rho\frac{dSV^2}{ds} + \rho hU^2\sin\Psi\cos\Psi, \tag{A2}$$

$$-\oint_\Sigma \rho\mathbf{v}(\mathbf{n}\cdot\mathbf{v})d\Sigma\frac{\mathbf{e}_N}{ds} = -\rho SV^2\frac{d\Psi}{ds} - \rho hU^2\sin^2\Psi. \tag{A3}$$

Then, (14) reads

$$\left.\frac{d\mathbf{p}}{dt}\right|_\Sigma\cdot\mathbf{e}_T = \rho ds\cos\Psi \times\left(gS + \frac{\gamma}{\rho}\frac{dl_r}{dz} - \frac{dSV^2}{dz} + hU^2\sin\Psi\right), \tag{A4}$$

$$\left.\frac{d\mathbf{p}}{dt}\right|_{\Sigma}\cdot\mathbf{e}_N=\rho ds\left(-gS\sin\Psi+\frac{2\gamma}{\rho}+\frac{\gamma l_r}{\rho}\frac{d\sin\Psi}{dz}-SV^2\frac{d\sin\Psi}{dz}-hU^2\sin^2\Psi\right). \tag{A5}$$

The purpose of the calculus is to find stationary solutions for the hole, so that $d\mathbf{p}/dt|_{\Sigma}=0$. Then, (A5) becomes

$$\begin{aligned}gS\sin\Psi+hU^2\sin^2\Psi&=\sin\Psi\frac{dSV^2}{dz}-\frac{\gamma}{\rho}\sin\Psi\frac{dl_r}{dz}\\&=\frac{2\gamma}{\rho}+\frac{\gamma l_r}{\rho}\frac{d\sin\Psi}{dz}-SV^2\frac{d\sin\Psi}{dz},\end{aligned} \tag{A6}$$

$$\begin{aligned}\frac{2\gamma}{\rho}+\frac{\gamma}{\rho}\sin\Psi\frac{dl_r}{dz}+\frac{\gamma l_r}{\rho}\frac{d\sin\Psi}{dz}&=\sin\Psi\frac{dSV^2}{dz}+SV^2\frac{d\sin\Psi}{dz}.\end{aligned}$$

Combining (3) with (13), it leads to

$$\frac{2\gamma}{\rho}+\frac{\gamma}{\rho}\frac{dl_r\sin\Psi}{dz}=\frac{d\dfrac{\Gamma^2x^2\sin\Psi}{S}}{dz}. \tag{A7}$$

Integrating the previous equation from the summit to x, one obtains

$$\frac{2\gamma}{\rho}\left[z+\frac{1}{2}l_r\sin\Psi-\left(z_0+\frac{1}{2}l_{b0}\sin\Psi_0\right)\right]=\frac{\Gamma^2x^2\sin\Psi}{S}. \tag{A8}$$

Values at the summit are denoted by the subscript 0.

At this stage, it is necessary to argue some simplifying assumptions: first, the term $\frac{1}{2}l_r\sin\Psi$ is at the most equal to the rim diameter (less than 2 mm). This is to be compared with z which varies over more than 10 cm. Furthermore, with the naked eye, it is clear that both l_r and ψ vary slowly compared to z. So, in the following, we neglect $\frac{1}{2}(l_r\sin\Psi-l_{b0}\sin\Psi_0)$ compared to $(z-z_0)$. This is to say that the rim is considered as a slender curve, on which each point is associated with the quantities S, V, and l_r. The value of z is then undetermined with an error of order of magnitude equal to the rim thickness. However this does not mean that the weight of the rim is neglected. Equation (A8) then becomes

$$\frac{2\gamma}{\rho}(z-z_0)=\frac{\Gamma^2x^2\sin\Psi}{S}=SV^2\sin\Psi. \tag{A9}$$

Reconsidering (A6), one can notice that SV^2 is much larger than $\gamma l_r/\rho$. Indeed, (A9) leads to

$$\frac{SV^2}{\dfrac{\gamma l_r}{\rho}}=\frac{2}{\sin\Psi}\frac{z-z_0}{l_r}>2\frac{z-z_0}{l_r}. \tag{A10}$$

As l_r is around 1 mm, $z-z_0$ is of the order of several centimeters, considering the extension of the hole. Then, the above ratio will be around 100. The term $\gamma l_r/\rho$ is then neglected in (A6). Nevertheless, we keep in mind that such approximations may be prevented from giving a realistic shape near the obstacle. Thus, replacing S and SV^2 by their expression as a function of x, z, and Ψ from (A9)

$$\frac{\rho g\Gamma^2}{2\gamma}\frac{x^2}{z-z_0}\sin\Psi+\Gamma U\sin\Psi=\frac{2\gamma}{\rho}\frac{d}{dz}\left(\frac{z-z_0}{\sin\Psi}\right). \tag{A11}$$

We can find here the expression of the transonic length $z^*=2\gamma^2/\rho^2g\Gamma^2$ [Eq. (8)]. Let us normalize all the lengths by z^*: $\tilde{z}=z/z^*$, $\tilde{z}_0=z_0/z^*$, and $\tilde{x}=x/z^*$. By replacing U by its value from Eq. (6), we finally obtain

$$\begin{aligned}\frac{\tilde{x}^2}{2(\tilde{z}-\tilde{z}_0)}+\sqrt{\tilde{z}}&=\frac{1}{\sin^2\Psi}+\frac{\tilde{z}-\tilde{z}_0}{\sin\Psi}\frac{d}{d\tilde{z}}\left(\frac{1}{\sin\Psi}\right)\\&=1+\left(\frac{d\tilde{z}}{d\tilde{x}}\right)^2+\frac{\tilde{z}-\tilde{z}_0}{2\dfrac{d\tilde{z}}{d\tilde{x}}}\frac{d}{d\tilde{x}}\left(\frac{1}{\sin^2\Psi}\right)\\&=1+\left(\frac{d\tilde{z}}{d\tilde{x}}\right)^2+(\tilde{z}-\tilde{z}_0)\frac{d^2\tilde{z}}{d\tilde{x}^2}.\end{aligned}$$

Dividing by $(\tilde{z}-\tilde{z}_0)$, one finally obtains (19).

[1] K. Miyamoto and Y. Katagiri, "Curtain coating," in *Proceedings of the Second European Coating Symposium, Strasbourg*, edited by Kistler and Schweizer (Chapman-Hall, London, 1997).
[2] A. H. Lefebvre, *Atomization and Sprays* (Hemisphere, New York, 1989).
[3] D. Soderberg and P. H. Alfredsson, "Experimental and theoretical stabilitiy investigations of plane liquid jets," Eur. J. Mech. B/Fluids **17**, 689 (1998).
[4] D. R. Brown, "A study of the behaviour of a thin sheet of a moving liquid," J. Fluid Mech. **10**, 297 (1961).
[5] F. E. C. Culick, "Comments on a ruptured soap film," J. Appl. Phys. **31**, 1128 (1963).
[6] G. I. Taylor, "The dynamics of thin sheets of fluids. I Water bells. II Waves on fluid sheets. III Disintegration of fluid sheets," Proc. R. Soc. London, Ser. A **253**, 289 (1959).
[7] C. Clanet and E. Villermaux, "Life of a smooth liquid sheet," J. Fluid Mech. **462**, 307 (2002).
[8] P. Brunet, C. Clanet, and L. Limat, "Transonic liquid bells," Phys. Fluids **16**, 2668 (2004).
[9] S. P. Lin and G. Roberts, "Waves in a viscous liquid curtain," J. Fluid Mech. **112**, 443 (1981).
[10] L. de Luca and M. Costa, "Instability of a spatially developing liquid sheet," J. Fluid Mech. **331**, 127 (1997).
[11] S. P. Lin, "Stability of a viscous liquid curtain," J. Fluid Mech. **104**, 111 (1981).
[12] S. P. Lin, Z. W. Lian, and B. J. Creighton, "Absolute and convective instability of a liquid sheet," J. Fluid Mech. **220**, 673 (1990).
[13] L. de Luca, "Experimental investigation of the global instability of plane sheet flows," J. Fluid Mech. **399**, 355 (1999).
[14] G. Sunderhauf, H. Raszillier, and F. Durst, "The retraction of the edge of a plane liquid sheet," Phys. Fluids **14**, 198 (2002).
[15] K. Adachi, T. Aoki, S. Nishida, and R. Nakamura, "A hydrodynamics investigation of a falling liquid film for curtain coating and sheet casting," in *Proceedings of the Tenth International Congress on Rheology* (Australian Society of Rheology, Sydney, 1988), Vol. 1, pp. 122–124.
[16] L. de Luca and M. Costa, "Stationary waves on plane liquid sheets falling vertically," Eur. J. Mech. B/Fluids **16**, 75 (1997).
[17] S. J. Weinstein, A. Clarke, A. G. Moon, and E. A. Simister, "Time-dependent equations governing the shape of a two-dimensional liquid curtain, Part 1: Theory," Phys. Fluids **9**, 3625 (1997).
[18] N. S. Clarke, "Two-dimensional flow under gravity in a jet of viscous liquid," J. Fluid Mech. **31**, 481 (1968).
[19] J. P. K. Tillett, "On the laminar flow in a free jet of liquid at high Reynolds numbers," J. Fluid Mech. **32**, 273 (1968).

[20]D. S. Finnicum, S. J. Weinstein, and K. J. Ruschak, "The effect of applied pressure on the shape of a two-dimensional liquid curtain falling under the influence of gravity," J. Fluid Mech. **255**, 647 (1993).
[21]S. J. Weinstein, J. W. Hoff, and D. S. Ross, "Time-dependent equations governing the shape of a three-dimensional liquid curtain," Phys. Fluids **10**, 1815 (1998).
[22]M. G. Antoniades, R. Goldwin, and S. P. Lin, "A new method of measuring dynamic surface tension," J. Colloid Interface Sci. **77**, 583 (1980).
[23]C. H. Teng, S. P. Lin, and J. N. Chen, "Absolute and convective instability of a viscous liquid curtain in a viscous gaz," J. Fluid Mech. **332**, 105 (1997).
[24]P. Luchini, "Is a plane liquid curtain algebraically absolutely unstable?," Phys. Fluids **16**, 2154 (2004).